

AERODYNAMIC ANALYSIS OF AN AXIAL FLOW TURBINE STAGE FOR A 5 kN TURBOJET ENGINE

Marco Aurélio B. Santin

ITA - Praça Marechal Eduardo Gomes, 50 - Vila das Acácias - São José dos Campos, SP - Brasil - 12228-900
marcoabs@ita.br

João Roberto Barbosa

ITA - Praça Marechal Eduardo Gomes, 50 - Vila das Acácias - São José dos Campos, SP - Brasil - 12228-900
barbosa@ita.br

Abstract. A stage of axial flow turbine is designed for the application in a gas turbine engine and its three-dimensional flow field is analyzed. The baseline turbomachinery is designed based on a mean line zero-dimensional approach. The off-design performance is predicted with a mean line methodology based on the loss correlations suggested by Ainley-Mathieson and Kacker-Okapuu and the axial turbine performance curves are generated. The 3-D blade geometry is established by using 3 and 5 arcs MCA profiles. A mesh of about 600,000 hexahedral elements is constructed and the solution is obtained for steady state by using periodic boundary conditions and a mixing plane for stator-rotor interaction. RANS equations with Spalart-Allmaras turbulence model are solved by using a commercial CFD software. The simulation in several operating points allowed the construction of the turbine performance curves, which were compared to those generated by using the correlations of Ainley-Mathieson and Kacker-Okapuu. The CFD results show that mass flow is under-predicted by the mean line methodology while efficiency and power are over-predicted.

keywords: Gas Turbines, Axial Flow Turbines, CFD, Turbojets, Turbine Performance Maps

1. Introduction

Worldwide gas turbine production amounted to a total of US\$25.6 billion in 2005 (Langston, 2006), demonstrating the importance of this engine nowadays. Most commercial and military aircrafts employ it for propulsion and auxiliary power generation, mainly thanks to its high power/weight ratio. The fundamental module that describes a gas turbine is constituted by compressor, combustor and turbine. The working fluid, usually air, enters the compressor and receives energy in a process of compression. In the combustor, more energy is added by burning the fuel. Turbine extracts from the combustion gases the energy necessary to drive the compressor. In a turbojet engine, after leaving the turbine, the flow passes through a nozzle creating the jet that propels the aircraft.

An axial turbine stage is composed by a stator followed by a rotor. The first one's function is to convert pressure energy into kinetic energy and to drive the flow towards rotor inlet. In this last one, a part of the flow energy is converted into shaft power.

The efficiency of the current turbines is usually over 90%, making further improvements more difficult to obtain. Advances are still possible, not only in efficiency, but by lowering the cost to obtain this performance, by a more precise comprehension of the flow physical characteristics (Denton, 1993). The application of CFD analysis in the main gas turbine components is in agreement with this philosophy as it makes possible to refine the design with a comparatively less expensive tool and to reduce the development work done in test rigs, resulting in lower design cost.

Until about 1940, the design of an axial flow turbine was based only on an one-dimensional point of view, by the velocity triangles. At the beginning of the 1950s, the blade-to-blade flow characteristics were well understood; even so, design was mainly based on correlations (Cumpsty and Greitzer, 2004). From the 1970s, two-dimensional calculation methods became widespread, like the *Actuator Disc* and *Throughflow* approaches, which solve the flow considering axial symmetry. The usage of CFD as a turbomachinery design tool began in the 1970s for two-dimensional solutions and passed then to three-dimensional Euler solutions, in the 1980s, and to Navier-Stokes, in the 1990s. These developments were stimulated by the work done by J. Denton in the UK, about 1975, using Euler models; by R. Ni in the USA, in 1982, and W. Dawes, in 1988, using Navier-Stokes models (Hirsch and Demeulenaere, 2003).

The main objectives of this work were to design an axial flow turbine for a turbojet, to obtain its performance map, using three-dimensional viscous CFD simulation, and to compare this map with those obtained by using a performance prediction methodology that applies the loss correlations of Ainley and Mathieson, 1952, and Kacker and Okapuu, 1982.

The CFD software employed in this work was FLUENT for Linux, version 6.2.16. ICEM CFD, version 5.1, was applied to generate geometries and computational meshes. Turbine design and performance prediction were obtained by

using codes developed at ITA, initially as a part of the work of Bringhenti, 2003 (related to whole engine performance) and after for the work of Jesus, 2003 (related to variable geometry turbines).

2. Turbine Design

The baseline turbomachinery was designed by using the code mentioned previously. It is based on a mean line zero-dimensional approach and properties are determined along the blade by using the free vortex method. This code was implemented following the design recommendations of Saravanamuttoo *et al.*, 2001. The losses at design point, and therefore the efficiency, were estimated by using the model of Ainley and Mathieson, 1952.

At the design point of the proposed turbojet engine, the turbine operating conditions are as follows:

Inlet total temperature:	1123 K
Outlet total temperature:	940.9 K
Inlet total pressure:	471,668 Pa
Mass flow:	8.34 kg/s

From compressor design, shaft rotational speed N was defined as 25,500 rpm. The blade tip velocity was limited to 400 m/s, for structural issues.

Several authors define criteria for evaluating an axial turbine design, as can be found in Mattingly, 1996; Wilson and Korakianitis, 1998; Saravanamuttoo *et al.*, 2001. It is recommended to ensure that stator outlet angle be less than 70° to avoid high deviation, which result in increased profile losses. When the absolute outlet angle of the last stage is high, it results in high losses in the nozzle, therefore it must be less than 20° . It is recommended to do not allow a loading factor greater than 1.8 at mean diameter, to avoid high losses. The relation between tip and hub radius must be less than 1.4, to avoid structural and assembly problems; but must be greater than 1.2 to avoid that tip losses become predominant. The angle of divergence between the walls must be less than 25° to avoid flow detachment on endwall. To avoid vibration, it is recommended that the stator-rotor spacing be greater than 20% of stator axial chord. It is imposed that reaction at hub be greater than zero to avoid recompression.

Turbine preliminary design characteristics are:

Stator with cylindrical hub and casing			
Rotor with cylindrical casing			
Stator blade number:	31	Reaction degree (mean diameter):	0.444
Rotor blade number:	41	Reaction degree (root):	0.153
Isentropic efficiency:	0.909	Expansion ratio:	2.2
Stator losses:	0.0578	Stator blade height:	34.3 mm
Rotor losses:	0.0755	Rotor outlet blade height:	42.7 mm
Rotor outlet relative Mach :	0.981	Casing radius:	149.7 mm
Loading factor:	1.658	Tip clearance:	0.0 mm
Flow coefficient:	0.843		

3. Performance Prediction

Off-design performance was predicted with the mean line methods suggested by Ainley and Mathieson, 1952, and Kacker and Okapuu, 1982, and the axial turbine performance curves were generated by an in-house developed software. The performance prediction methodology implemented by Jesus, 2003, is a modification of the methodology suggested by Ainley and Mathieson, 1952; which estimates efficiency by calculation of *loss coefficients*.

Losses are any phenomena that reduce turbine efficiency, which can be associated to viscous friction, non equilibrium process and heat transfer across finite temperature differences (Denton, 1993). The loss coefficient Y can be related to pressure losses by Eq.(1), where the subscripts i and o indicate cascade inlet and outlet, respectively.

$$Y = \frac{P_{ti} - P_{to}}{P_{ti} - P_o} \quad (1)$$

Frequently, the losses related to distinct phenomena are modeled separately and are then combined to result in a total loss. The form of how this division is made is not a consensus between different authors, but generally there are: *profile losses*, related to blade boundary layer, detachment, wake and shock waves; *clearance losses*, related to flow leakage over the tips of rotor blades and the hub clearance of stator blades; and *secondary losses*, related to secondary flow and to endwall boundary layer. The contribution of these components can vary from a turbomachinery to another, but in most machines each one contributes with a third part of the total loss.

The loss method of Ainley and Mathieson, 1952, is based on experimental data of turbines of the 1950s and was widely used since then. In this method it is assumed that the losses are not influenced by the flow Mach number and that exit flow angle is not influenced by the incidence angle. The total loss coefficient Y is calculated by Eq.(2), where Y_P

is related to profile losses; Y_T is related to clearance losses; Y_S is related to secondary losses and $f(t_{te})$ is a function of trailing edge thickness.

$$Y = (Y_P + Y_S + Y_T) f(t_{te}) \tag{2}$$

The loss method of Kacker and Okapuu, 1982, is a modernization of the method of Ainley-Mathieson. The difference from de former is the structure of the loss system and the introduction of compressibility and shock waves influences (Wei, 2000). The total loss coefficient for this method is calculated by Eq.(3), where $f(Re)$ is a function of Reynolds number and the part of the profile losses related to wake is accounted by *trailing edge losses* Y_{te} .

$$Y = f(Re) Y_P + Y_S + Y_T + Y_{te} \tag{3}$$

The off-design performance simulation code, which includes these two methods, was used to predict the behavior of the designed turbine. Results provided by the design code, allied to geometrical data of the blade at mean diameter, were inserted into the performance code. The performance of the turbojet turbine was predicted for 14 operating points, seven for 100% and seven for 80% of the design speed N , varying outlet pressure.

4. CFD Simulation

The test case DLR cascade, presented in AGARD-AR-355 report (Dunham, 1998), was studied with purpose of familiarization with the problem of turbine cascade simulation and to evaluate the applied methodology. This cascade is an annular turbine stator with cylindrical hub and casing tested by the German Aerospace Research Center, DLR. Workgroup 26 from AGARD compared DLR’s experimental data to several CFD simulations from different research groups. Flow data at cascade outlet were measured using a 5-hole probe and a 3D laser-two-focus (3D-L2F). The simulation done for the work here presented is more deeply described in Santin, 2006. Some of the results for circumferentially averaged values at cascade outlet are presented in Fig. (1).

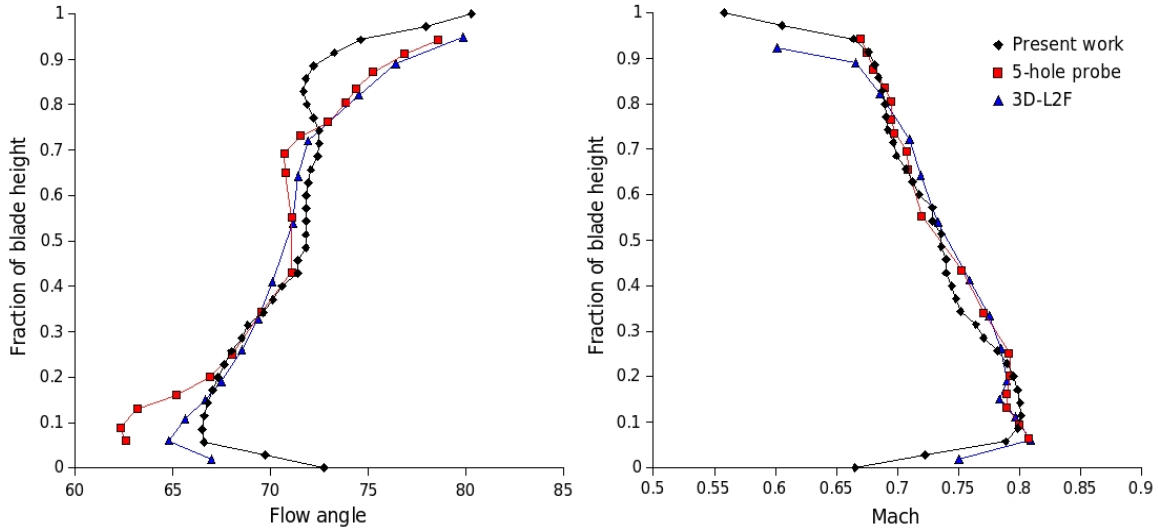


Figure 1: Circumferentially averaged values of cascade outlet flow angle and Mach number.

The CFD simulation methodology used in this work was chosen due to its feasibility on a personal computer. Aiming at the low computational cost, the turbine was simulated by the solution of RANS equations with Spalart-Allmaras turbulence model (Spalart and Allmaras, 1992), at steady state, using periodic boundary conditions and a mixing plane for the stator-rotor interaction.

The solver uses the finite volume method with second-order upwind scheme, is coupled, explicit, and uses one level of FAS (*Full-Approximation Storage*) multigrid to accelerate convergence (further details can be found in Fluent Inc., 2003).

The Spalart-Allmaras turbulence model is based on the Boussinesq hypothesis and uses one equation to solve the turbulent viscosity. As it includes only one more equation, it is seen as a low computational cost model. An analysis of the application of turbulence models to cascades is shown in Dunham, 1998. This model showed acceptable performance for obtainment of global parameters. It also showed good performance in regions of adverse pressure gradient (Menter, 2003). The turbulence model implemented in this solver does not account for the boundary layer transition (Fluent Inc., 2003), therefore in all operating points the flow was considered fully turbulent.

The turbine was simulated as a single channel of stator plus a single channel of rotor, supposing that flow properties in other channels of the row are similar. This consideration difficults the prediction of the real phenomenon, mainly in the

rotor, but should be sufficiently accurate for the construction of a performance map. The domain is then reduced to 1/31 for the stator and to 1/41 for the rotor, what reflects in a similar reduction of the computational cost .

The choice of steady state simulation neglects the unsteady phenomena related to stator-rotor interaction. These phenomena affect turbine performance, but it is supposed that time averaged properties are similar to that obtained in a steady simulation. By using the mixing plane model, total pressure, total temperature, turbulent viscosity and flow direction at stator outlet are circumferentially averaged and used as rotor inlet boundary condition. Similarly, static pressure at rotor inlet is circumferentially averaged and applied as stator outlet boundary condition.

Average Mach number of the studied cases is around 0.6 and usually assumes supersonic values at cascade outlet, evidencing the importance of the effects of compressibility. The density variation was obtained by using ideal gas model and the temperature distribution was determined by solving the energy equation.

A great part of the losses is due to the tip clearance of the rotor, however it was not considered and its influence on the turbine performance map will be evaluated in a future work.

The blade geometry is established by an in-house developed software capable of designing 3 and 5 arcs MCA profiles. A group of computational tools makes possible to generate and change reasonably easily the blade geometry and mesh. This automated procedure is obtained via scripts, which are read by ICEM CFD. This is a manner to reduce the turn-around time of this phase that is usually long. The details of the domain are presented in Fig. (2).

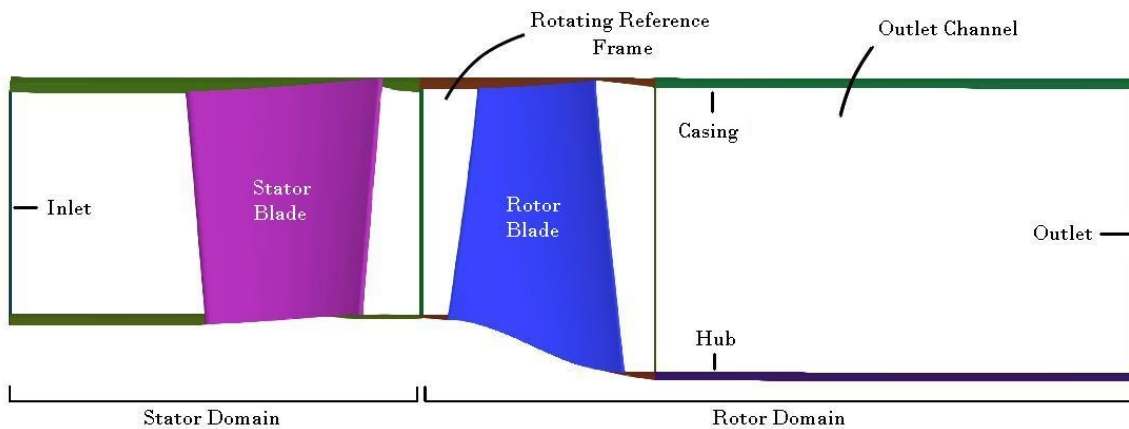


Figure 2: Computational domain used for the simulation of the turbine stage.

The mesh generated for this study presents 584,288 cells (276,830 in the stator, 196,230 in the rotor and 111,228 in the outlet channel) and is composed by 29 blocks (13 in the stator, 13 in the rotor e 3 in the outlet channel). Mesh quality was verified initially by its values of minimum angle of 28.2° , minimum determinant of 0.52, maximum aspect ratio of 2.28 and minimum volume of $4,1 \cdot 10^{-12} \text{ m}^3$.

For solid surfaces, the boundary condition was set for null heat transfer and no slip. The fluid inside the rotor channel was set as a rotating reference frame and rotor blade and hub were set as moving walls (seen as static by the rotating frame). Outlet boundary condition was defined by setting the static pressure at hub and distributing along the height by Eq. (4) of radial equilibrium, where v_t is tangential flow velocity, ρ is density and r is radial position.

$$\frac{1}{\rho} \frac{dP}{dr} = \frac{v_t^2}{r} \quad (4)$$

The inlet boundary condition was defined with constant values of total pressure, total temperature, static pressure (for initial calculation) and turbulent intensity. The influence of the turbulent intensity is important, but depends on upstream information, unknown at this phase of the engine design. Therefore, a value of 5% was established based on the value used by Dunham, 1998. The settings for the inlet boundary condition was the following:

Total pressure:	472 kPa
Total temperature:	1123 K
Flow direction:	axial
Static pressure (initial):	440 kPa
Turbulence intensity:	5%
Hydraulic diameter:	0.0061 m

Fourteen cases were studied; seven for 100%N and seven for 80%N, changing the pressure at the outlet boundary condition (pressure at the hub). The operating points (OP) that were evaluated are presented in Tab. (1).

The inlet measuring plan (section 1) was positioned at a distance from the stator leading edge of 0.3 times its axial chord; while the outlet measuring plan (section 3) was positioned at a distance from the rotor trailing edge equal to 1.2 times its axial chord.

Table 1: Operating points simulated by CFD

OP	0	1	2	3	4	5	6	7	8	9	10	11	12	13
Pressure at Outlet (<i>kPa</i>)	120	180	220	250	280	320	360	120	180	220	250	280	320	360
Speed (<i>rpm</i>)	25,500 (100% <i>N</i>)							20,400 (80% <i>N</i>)						

The power W of the axial turbine was calculated from total enthalpy H_t drop in the flow along an adiabatic process by Eq. (5), where n_B is number of blades, v_a is axial velocity, A is cross section area, and the subscripts I and O indicate turbine inlet and outlet, respectively.

$$W = H_{tI} - H_{tO}, \quad \text{where} \quad H_t = n_B \int \rho v_a h_t dA \quad (5)$$

Turbine efficiency was calculated from the relation between real and ideal powers. The ideal power is given by the total enthalpy drop along an isentropic process. The temperature drop along this isentropic process for an ideal gas can be represented by the Eq. (6), where a_1, a_2, a_3 e a_4 are the constants of a specific heat polynomial variation with temperature of third order.

$$a_1 \ln \left(\frac{T_{tOs}}{T_{tI}} \right) + a_2 (T_{tOs} - T_{tI}) + \frac{a_3}{2} (T_{tOs}^2 - T_{tI}^2) + \frac{a_4}{3} (T_{tOs}^3 - T_{tI}^3) - R \ln \left(\frac{P_{tO}}{P_{tI}} \right) = 0 \quad (6)$$

Outlet isentropic total temperature T_{tOs} can be obtained numerically, based on mean properties at inlet and outlet. Therefore, outlet total enthalpy in an isentropic process is calculated by Eq. (7), where \dot{m} is the mass flow.

$$H_{tOs} = \dot{m} h_{tOs}, \quad \text{where} \quad h_{tOs} = a_1 T_{tOs} + \frac{a_2}{2} T_{tOs}^2 + \frac{a_3}{3} T_{tOs}^3 + \frac{a_4}{4} T_{tOs}^4 \quad (7)$$

5. Results and Discussions

The simulations demanded 770 MB of RAM and the average time per iteration was 24.7 s with an Intel Pentium 4 HT 2.4 GHz processor. The first case demanded 4300 iterations and the subsequent cases were obtained from this after 3000 more iterations each.

The convergence was detected by the stabilization of the mass flow. The difference between the inlet and the outlet mass flow was no more than 0.02% \dot{m} (with oscillation of 0.05%) for the stator and no more than 0.01% \dot{m} (with oscillation of 0.1%) for the rotor.

The average values of y^+ obtained with the simulation were no more than 64, and on most parts of the blade the values were close to the 50, which is adequate for the application of wall functions.

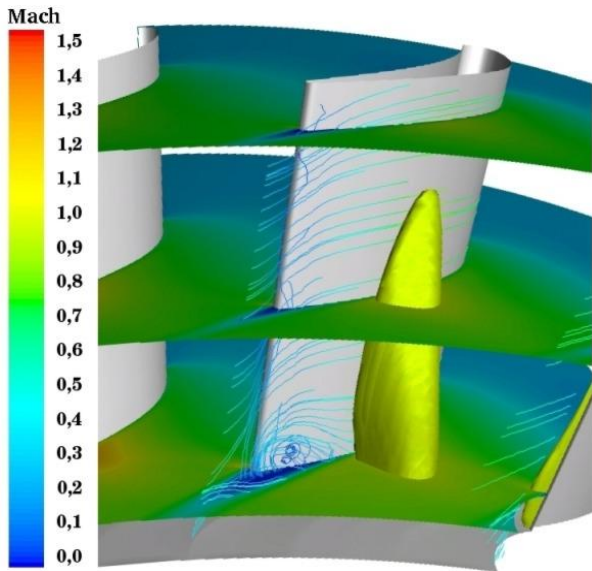


Figure 3: Mach distributions in the stator at OP 1.

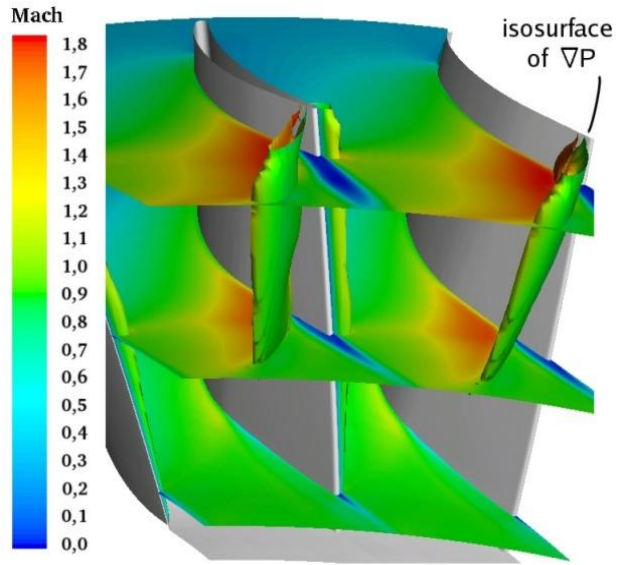


Figure 4: Mach distributions in the rotor at OP 1.

The main flow characteristics in the stator are shown in Fig. (3). The Mach number contours are shown on three surfaces along the blade height and on an isosurface of Mach equal to 1. There are also path lines originated close to the suction side of the blade. The main flow characteristics in the rotor are shown in Fig (4), with similar Mach number contour surfaces along the blade height and with an isosurface indicating high values of pressure gradient.

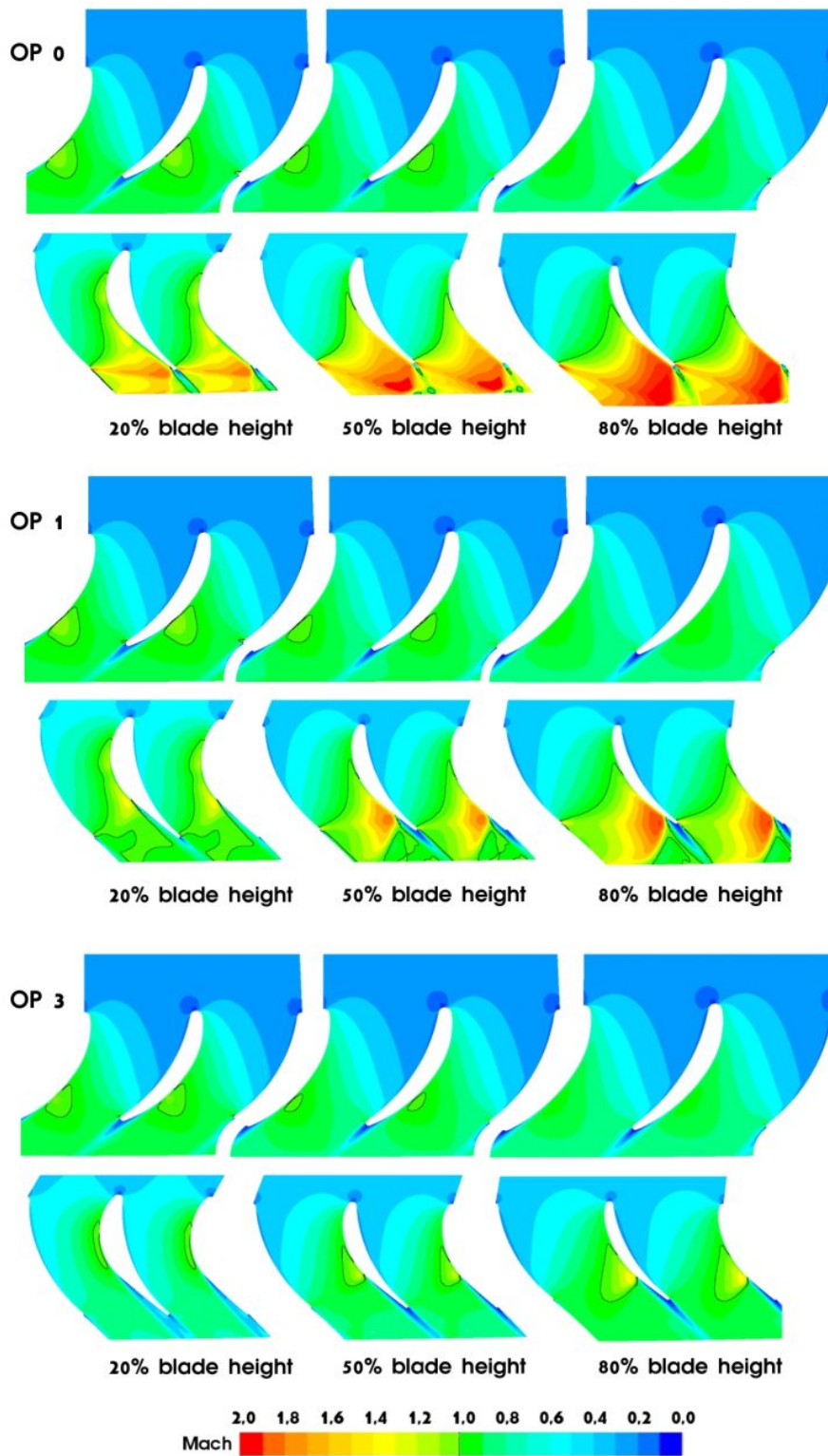


Figure 5: Contours of Mach on stator and relative Mach on rotor at OP 0, OP 1 and OP 3.

Figure (5) shows contours of Mach number on stator and relative Mach number on rotor at OP 0, OP 1 and OP 3. Rotor relative Mach numbers are much higher than stator absolute Mach numbers, which allows concluding that the stage choke initiates at rotor. From the point that the rotor is choked, the flow in stator stabilizes and alterations only occur at rotor outlet region.

At high expansion ratios, the fluid enters the stator at subsonic velocities, Mach around 0.3, and accelerate creating a supersonic region close to hub on the suction side rear portion that can reach Mach 1.2. On the corner between hub and suction side there is a region of boundary layer detachment. In this region, as can be seen in Fig. (6), occur an increase of static temperature, specific entropy and turbulent viscosity; occur a decrease of density and also a variation of radial velocity.

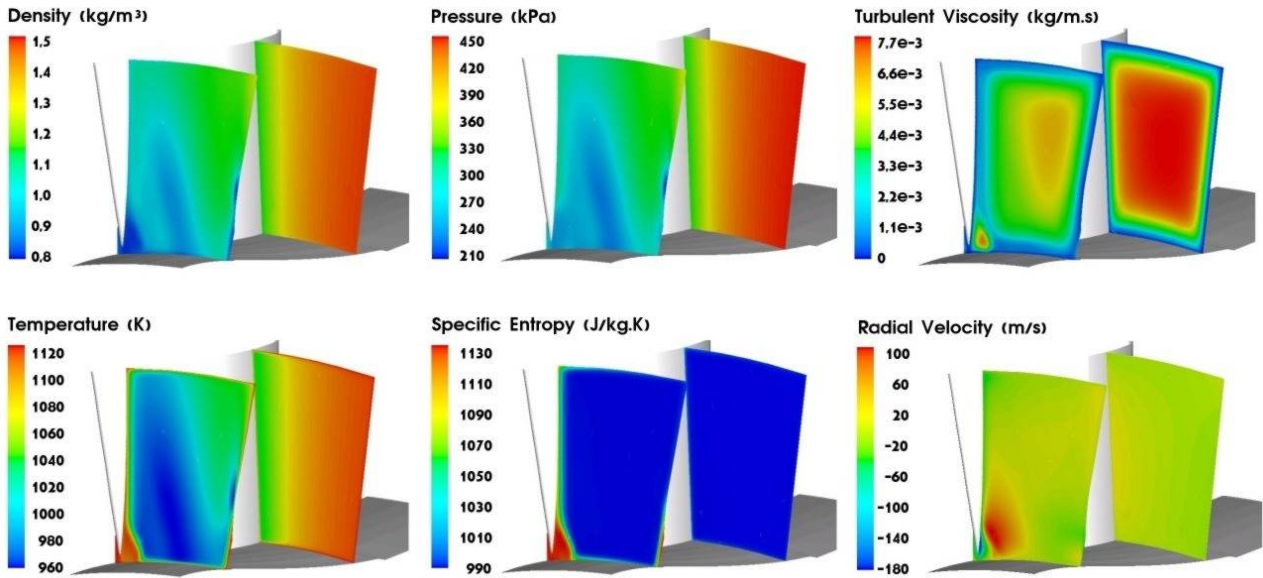


Figure 6: Rear view of the cross section contours in the stator at OP 1.

The flow enters the rotor at Mach numbers no more than 0.5 and reaches supersonic conditions in all operating conditions but those of lower expansion ratios. As the expansion ratio increases, the choke starts at tip and goes down the blade, as can be seen in Fig. (5). A shock wave arises at suction side and is followed by boundary layer detachment, caused by the adverse pressure gradient of the wave. The fluid from the hub goes up in this detachment region, leaving the blade in trailing edge vortices close the tip. As the expansion ratio increases, the shock wave moves toward the trailing edge of the suction side, reducing the detachment region. Fig. (7) illustrates wake and vortex formation at rotor trailing edge, indicated by regions of high static temperature, specific entropy and turbulent viscosity.

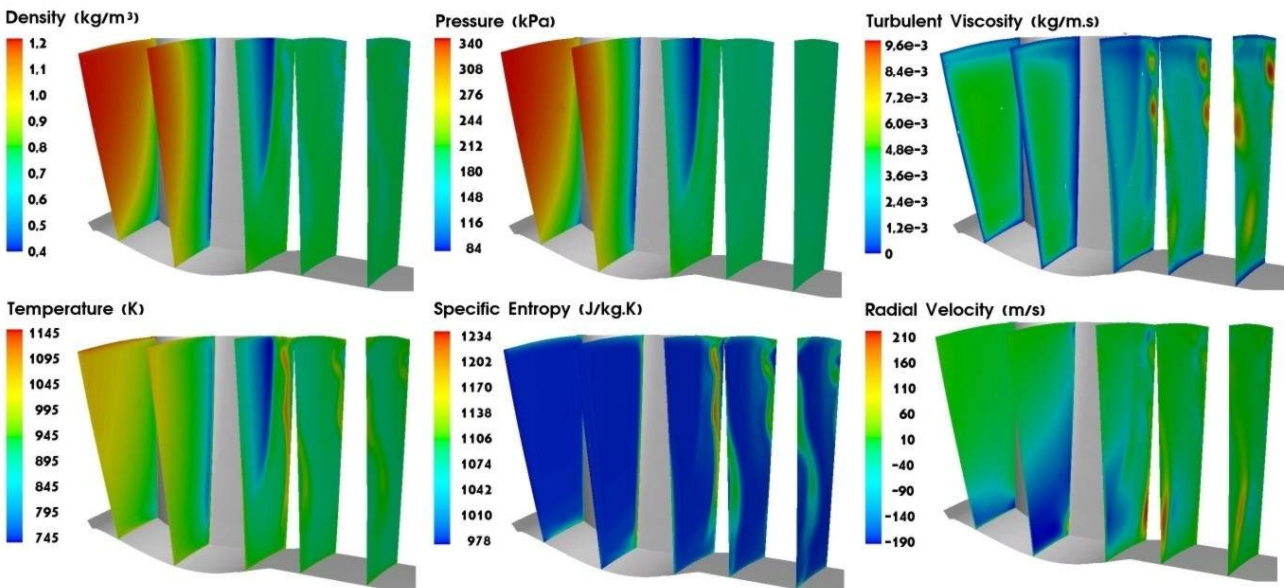


Figure 7: Rear view of the cross section contours in the rotor at OP 1.

Circumferentially averaged values of stator inlet angle and rotor inlet and outlet relative angles are shown in Fig. (8). The results indicate that stator flow deviation is approximately constant (around 10°) along the upper half of the blade, increasing on the bottom half due to boundary layer detachment on the trailing edge. Close to the tip, it is possible to

notice a decrease of deviation, probably related to the endwall boundary layer. The incidence is below 5° on a great portion of the blade height, achieving the design expectation. Due to relative motion, as mass flow decreases, incidence decreases; and as rotational speed decreases, incidence increases. The influence of the stator detachment can be clearly noticed on the bottom portion of the rotor leading edge, as it causes negative angles of incidence. Rotor flow deviation at mean height is around 8° , but can reach 15° in some regions. The deviation is high on tip due to the endwall boundary layer that is stationary in the absolute reference frame. At root there is a strong secondary flow from pressure side to suction side, resulting in high angle values.

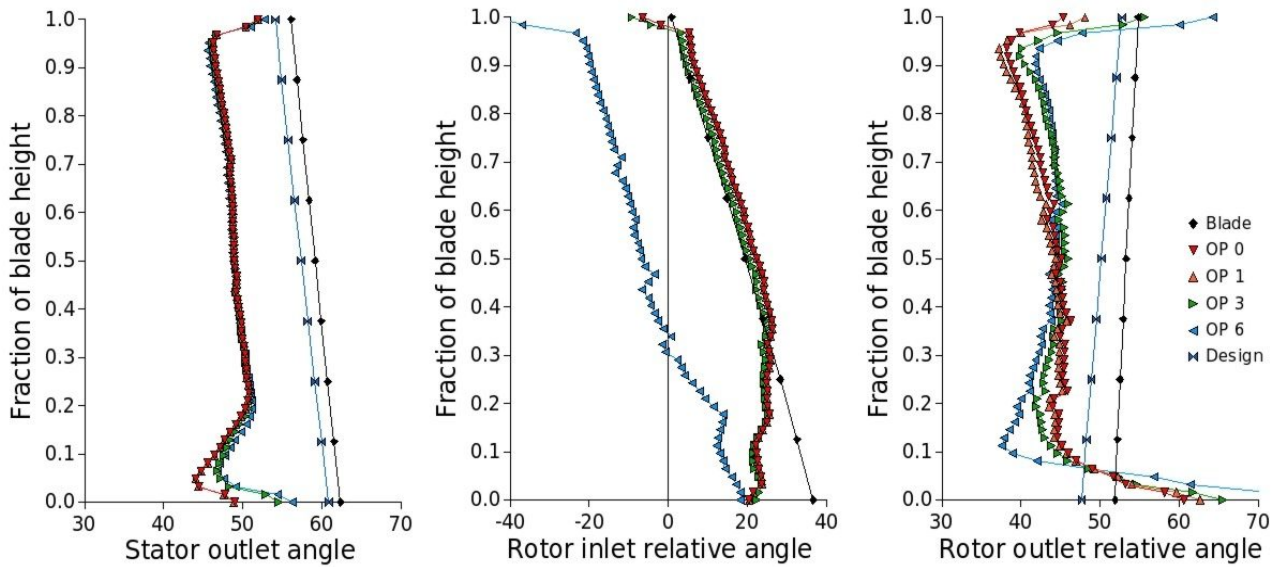


Figure 8: Circumferentially averaged values of stator inlet angle and rotor inlet and outlet relative angles.

Total enthalpy development along the axial length is shown in Fig. (9) for several operating points. From the first law of thermodynamics, total enthalpy must remain constant in adiabatic processes without work transference and must decrease when work leaves the control volume. The data show that there are small oscillations along the domain, probably due to numerical uncertainties. In a region just after the rotor, these oscillations become noticeable, mainly at OP 0. This effect can be related to the high gradients associated to the shock waves that can produce errors due to poor refinement. At OP 6, total enthalpy is increased close to rotor leading edge, what is probably caused by the poor flow incidence, as was shown in Fig. (8). There is a small leap of total enthalpy when crossing the mixing plane, caused by uncertainty on passing flow informations from one domain to other.

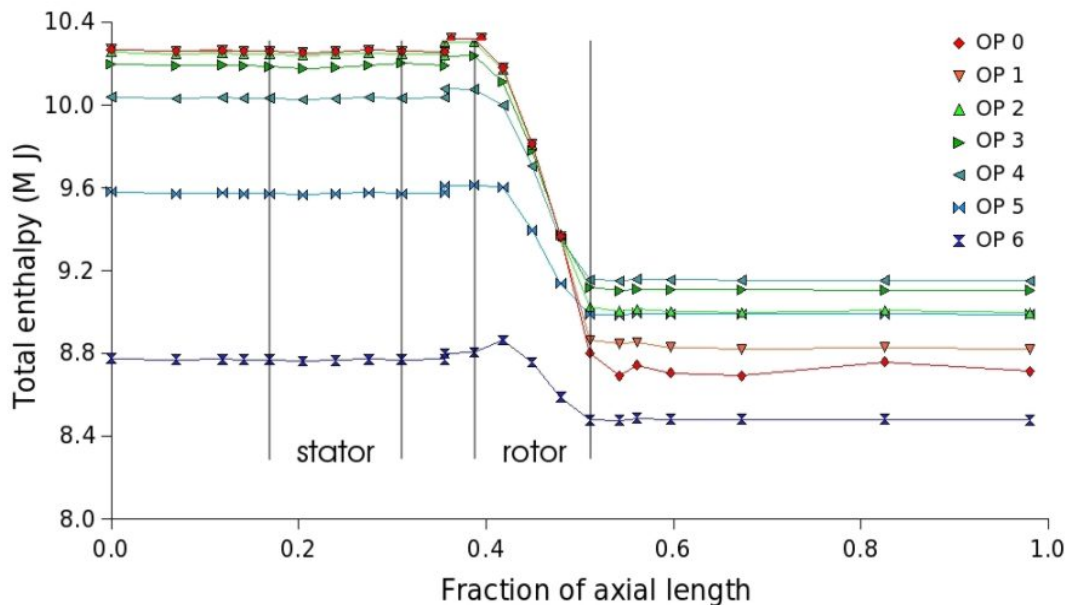


Figure 9: Total enthalpy along the axial length.

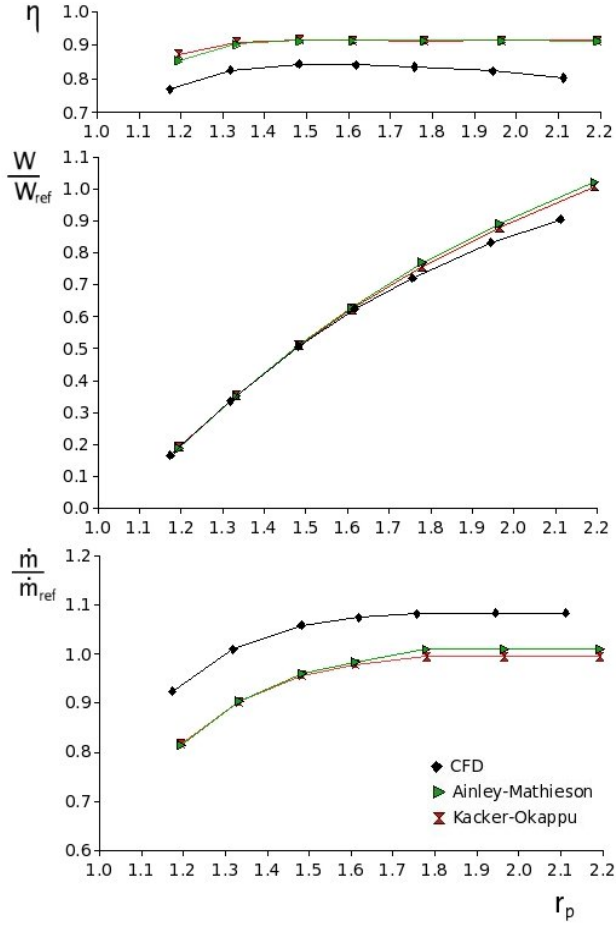


Figure 10: Performance map of the turbine for 100% N.

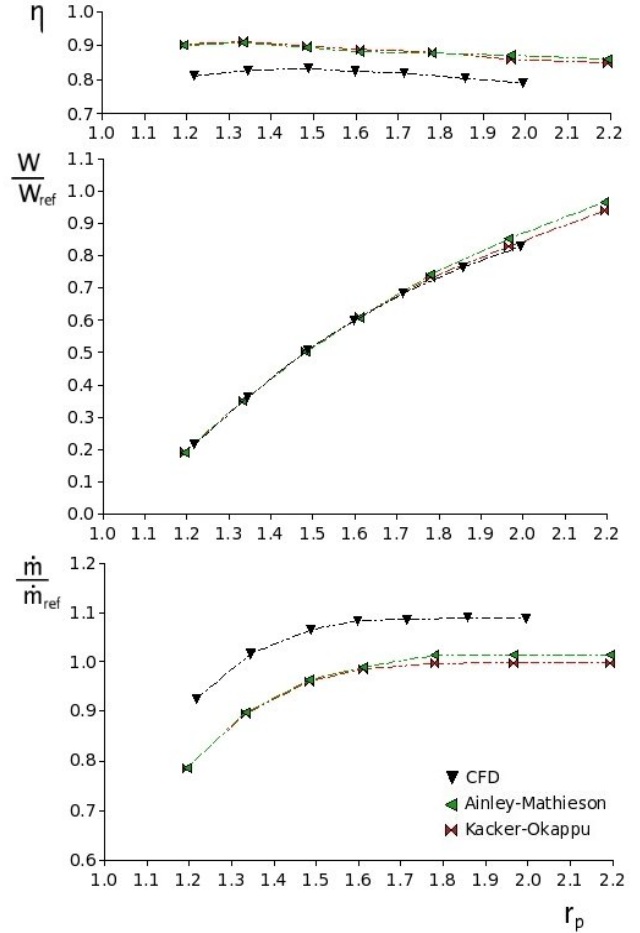


Figure 11: Performance map of the turbine for 80% N.

The performance maps obtained by CFD simulation and by using the mean line methodology are presented in Fig. (10) and Fig. (11), for 100% and 80% of the design speed, where η is efficiency. Non-dimensional power and mass flow were obtained by dividing the calculated values by the design values of power W_{ref} and mass flow \dot{m}_{ref} . The choking was established when the mass flow variation was reduced below $0.5\% \dot{m}$. The results of the CFD simulation indicate agreement with the results obtained by using the mean line methodology concerning the expansion ratio that occurs choking.

At choke region, the mass flow obtained by CFD was 8.3% greater than the design mass flow for 100%N and 8.7% greater for 80%N, what is probably caused by the error of mean density estimation in the area calculation of the mean line design approach.

The efficiency predicted by CFD is noticeably lower than that obtained by using the loss correlations of Ainley-Mathieson and Kacker-Okapuu. At an expansion ratio of 2, for 100%N, the differences in efficiency were in order of 10%.

The power predicted by CFD also is lower than the obtained by using the loss correlations; however the differences are not as great as those of the efficiency due to the greater mass flow of the CFD simulations.

By using Eq. (8) from Kacker and Okapuu, 1982, the efficiency reduction due to the presence of a tip clearance can be calculated. The parameter h_B is blade height and k is tip clearance. Supposing a tip clearance of 1mm, the efficiency would be reduced by 0.045.

$$\Delta\eta = 0,93 \left(\frac{r_{tip}}{r_{mean}} \right) \left(\frac{\Delta k}{h_B \cos\alpha_s} \right) \eta_{(k=0)} \quad (8)$$

6. Concluding Remarks

A commercial CFD software was employed on the analysis of the flow in an axial turbine for a gas turbine engine. The performance maps of the turbine were generated and compared to the maps generated by using a mean line methodology for performance prediction that uses the loss correlations of Ainley-Mathieson and Kacker Okapuu.

The test case *DLR Cascade* of AGARD AR-355 report was simulated to familiarize with the study of flows in turbine cascades and to evaluate the methodology employed. The results indicate a good representation of the physical phenom-

enon that was measured. In global terms, the values of the properties agree with the measurements, even if there are some local discrepancies.

The CFD simulation of the axial turbine indicates that the mass flow calculated by the mean line methodology was underestimated. By the use of the Ainley-Mathieson and Kacker-Okapuu correlations, the mean line methodology lead to overestimate power and efficiency.

The softwares for design and performance prediction of axial flow turbines are essential tools for its preliminary design, even if these methodologies present the deficiencies of a zero-dimensional modeling. At this initial phase, the design must be redone hundreds or thousands of times, evidencing the necessity for simpler models. The employment of the CFD simulations is interesting at a second design phase, in which the redesign times are larger, giving good quantitative informations of the flow field and indicating regions where the loss generation is undesirably high. To seek the improvement of the precision of the preliminary design tools is important to avoid the usage of CFD simulations to correct global problems of the design.

7. Acknowledgements

The authors thank CAPES (*Coordenação de Aperfeiçoamento de Pessoal de Nível Superior*) for the support to the research on gas turbine, developed at the *Centro de Referência em Turbinas a Gás* with support of ANEEL projects. Thanks also to Genival Sena de Jesus for the assistance with the design and performance softwares.

8. References

- Ainley, D. G. and Mathieson, G. C. R., 1952, A Method of Performance Estimation for Axial-Flow Turbines, Technical Report R.111, NTGE.
- Brighenti, C., 2003, “Variable Geometry Gas Turbine Performance Analysis”, Ph. d., Instituto Tecnológico de Aeronáutica, São José dos Campos.
- Cumpsty, N. A. and Greitzer, E. M., 2004, Ideas and methods of turbomachinery aerodynamics: a historical view, “Journal of Propulsion and Power”.
- Denton, J. D., 1993, Loss Mechanisms in Turbomachines, “The 1993 IGTI Scholar Lecture”.
- Dunham, J., 1998, CFD Validation for Propulsion System Components, Technical Report AR-355, AGARD.
- Fluent Inc., 2003, FLUENT 6.1 User’s Guide.
- Hirsch, C. and Demeulenaere, A., 2003, State of the art in the industrial CFD for turbomachinery flows, “QNET-CFD Network Newsletter”.
- Jesus, G. S., 2003, Projeto e Análise de Desempenho de Turbinas Axiais de Vários Estágios com Geometria Variável, M. sc., Instituto Tecnológico de Aeronáutica, São José dos Campos.
- Kacker, S. C. and Okapuu, U., 1982, A Mean Line Prediction Method for Axial Flow Turbine Efficiency, “Journal of Engineering for Power”.
- Langston, L. S., 2006, Wild Blue Yonder, “Mechanical Engineering, Focus on Power and Energy”, Vol. 128, No. 5.
- Mattingly, J. D., 1996, “Elements of Gas Turbine Propulsion”, McGraw-Hill.
- Menter, F. R., 2003, Turbulence Modelling for Turbomachinery, “QNET-CFD Network Newsletter”.
- Santin, M. A. B., 2006, Simulação Numérica de Escoamento em Turbinas Axiais de Alto Desempenho, M. sc., Instituto Tecnológico de Aeronáutica, São José dos Campos.
- Saravanamuttoo, H. I. H., Rogers, G. F. C., and Cohen, H., 2001, “Gas Turbine Theory”, Prentice Hall, 5 edition.
- Spalart, P. R. and Allmaras, S. R., 1992, A One-Equation Turbulence Model for Aerodynamic Flows, “AIAA - 30th Aerospace Sciences Meeting and Exhibit”, AIAA-92-0439.
- Wei, N., 2000, “Significance of Loss Models in Aerothermodynamic Simulation for Axial Turbines”, PhD thesis, Royal Institute of Technology.
- Wilson, D. G. and Korakianitis, T., 1998, “The design of high-efficiency turbomachinery and gas turbines”, Prentice-Hall, EUA, 2 edition.